Microwave processing controls morphology of block copolymer templated mesoporous cobalt oxide films

Journal:	*Langmuir*
Manuscript ID	la-2019-03138u.R3
Manuscript Type:	Article
Date Submitted by the Author:	19-Jan-2020
Complete List of Authors:	Xia, Xuhui; University of Akron Vogt, Bryan; Pennsylvania State University, Chemical Engineering

Microwave processing controls morphology of block copolymer templated mesoporous cobalt oxide films

Xuhui Xia[1] *and Bryan D. Vogt*[2*]

[1]Department of Polymer Engineering, University of Akron, Akron, OH 44325

[2]Department of Chemical Engineering, The Pennsylvania State University, University Park, PA 16803

KEYWORDS. metal oxide, nanoporous, inductive heating, rapid thermal processing, crystallization

ABSTRACT: Microwave heating provides an efficient method to rapidly heat materials through interaction of microwaves with the media. Here we demonstrate the rapid synthesis of mesoporous cobalt oxide films through the heating of the silicon substrate by microwaves. A non-sol-gel approach based on cobalt nitrate-citric acid complex cooperative assembly with poly[methoxy poly(ethylene glycol)methacrylate]-block-poly(butyl acrylate) (PMPEGMA-b-PBA) block copolymer was used to fabricate the cobalt oxide through a cobalt carbonate intermediate. The time required to convert cobalt carbonate to cobalt oxide with the full removal of PMPEGMA-b-PBA template can be decreased by two orders of magnitude with microwaves in comparison to standard heating in a furnace at 350 ºC. At the highest microwave power examined (1500 W), this

can be accomplished within 2 s, while > 5 min is required at 350 ºC in a furnace. At microwave power < 400 W, there is insufficient energy to induce the transition from carbonate to oxide, but even at only 420 W the oxide can be formed within 26 s. The rapid heating by the microwaves tends to increase the crystallinity and mean crystal size of the cobalt oxide within the mesoporous films. Despite the growth of larger average crystals, the pore size and porosity tends to be larger when the film is processed using microwaves, with higher microwave power leading to larger average crystals and average pore size. These results suggest that rapid processing to crystallize frameworks in mesoporous materials may allow for highly crystalline frameworks without loss of the mesostructure.

INTRODUCTION

From the initial reports of surfactant templated ordered mesoporous silicates,[1-2] there has been significant interest in developing efficient and facile synthesis methods to expand the diversity of these materials in terms of framework chemistry,[3-4] pore size,[5-6] and ordered morphologies.[7] This expansion in the types of ordered mesoporous materials available has enabled the investigations into the suitability of these material frameworks for a diverse set of applications that can take advantage of their high surface area and interconnected structures, including drug delivery,[8] catalysis,[9-10] separations,[11] energy generation and storage.[12-14] The thin film form factor for these mesoporous materials is beneficial for a variety of potential applications. For example, mesoporous metal oxide thin films provide high surface area along with fast electrical response for gas sensors.[15-17] Grid-like mesoporous TiO_2 thin films are highly efficient photocatalysts for the degradation of undesired organic species in aqueous environments.[18] These ordered

mesoporous materials are most commonly fabricated by hard or soft templating.[19-20] Soft templating uses amphiphilic molecules to direct the mesostructure via self-assembly, while hard templating employs a preformed porous material to define the porous mesostructure. Though hard templating using mesoporous silica or carbon provides an approach to improved control over structure of the products, increased time and costs associated with inorganic template synthesis and removal are thought to limit its efficiency. Soft templating provides efficiency and convenience in the simple thermal removal of the soft template, but the low thermal stability of soft templates and need for multiple components to simultaneously assemble into the ordered structure can limit its applicability to some systems.

To improve the efficiency for the synthesis of mesoporous materials, a variety of different techniques have been examined to accelerate different aspects of the synthetic process. For example, alternative methods to remove the template have been explored through solvent extraction[21] or UV-ozone degradation.[22] These methods tend to help to retain the desired mesoporous structure. One common synthetic strategy is the use of microwaves to accelerate the reactions, generally through hydrothermal means, to decrease the reaction time from days or hours to minutes.[23-25] Microwaves have been used to accelerate the fabrication of cobalt oxide, but these processes tend to require both microwave and conventional furnace heating steps.[26,27] In one case, an initial microwave hydrothermal process (10 min) was followed by several conventional heating steps to obtain the mesoporous cobalt oxide materials,[26] while Luo *et al.* used microwaves (3 min) to generate a cobalt hydroxide intermediate that could subsequently be converted to oxide.[27] For other materials, microwave have been shown to be effective for calcination of mesoporous materials to decrease processing time from hours to minutes.[28] In addition to accelerating the synthesis, microwaves also can impact the morphology developed[29] with increased surface area

with highly crystalline frameworks,[30-31] potential for increased porosity,[32] and controlled surface chemistry[33] reported. As the heating with microwaves tends to be more uniform, the materials obtained tend to have less defects.[29]

Typically in order to decrease the potential for collapse of the mesostructure for crystalline frameworks, the amorphous framework formed from sol gel processing is commonly extensively aged to improve the mechanical robustness prior to crystallization,[34-36] Larger block copolymer templates produce materials are more tolerant of crystallization of the framework.[37] Alternative strategies that employ a template that *in-situ* provides a hard template can produce ordered mesoporous materials with highly crystalline frameworks.[38] There is evidence that microwaves can facilitate crystallization without the collapse of the mesostructure without the need for long aging times.[31, 39] A non-sol gel route to a variety of metal oxides and metal carbonates was developed by Eckhardt *et al.* based on metal nitrate-citric acid complex that progresses through a metal carbonate intermediate.[40-41] This route is advantageous for its ability to use low cost precursors in comparison to metal alkoxides and the sol is non-reactive under ambient conditions. However, the metal nitrate-citric acid complex route imposes limitations on the template as the complex is modestly hydrophobic and significant volume change between the precursor and the oxide could lead to structural collapse.[42] Common commercial templates such Pluronic F127 do not lead to mesoporous materials with this metal nitrate-citric acid complex.[40-41] Thus, custom block copolymer templates are typically required for the synthesis of mesoporous materials. Interestingly, this route was able to produce highly crystalline mesoporous manganese oxide films through microwave processing of the carbonate while maintaining the mesostructure, while calcination in a furnace led to much lower crystallinity and loss of the ordered mesostructure.[39] The increased crystallinity was attributed to the rapid heating by the microwaves and the direct

coupling of the microwaves to the Mn to locally provide energy. In this case, growth of the crystals ceased after 45 s of microwave irradiation, which limits the overall crystallinity. Routes to tune the crystals within mesoporous films using microwaves were not explored.

Here, the ability to use microwaves to tune the morphology of micelle-templated mesoporous cobalt oxide films using rapid microwave heating is systematically investigated as a function of both microwave power and processing time. These two factors influence the pore texture and crystal characteristics of the mesoporous cobalt oxide films. Microwave power can be used to precisely control the critical heating time required for the conversion of cobalt carbonate into cobalt oxide and full removal of the poly[methoxy poly(ethylene glycol)methacrylate]-block-poly(n-butyl acrylate) (PMPEGMA-b-PBA) template. The window for this conversion and template degradation is less than 1 s for microwave conditions. At insufficient power (<420 W), both the template and carbonate phase remain after 3 min of microwave exposure, while at 420 W, the critical heating time is 26 s and this time is decreased to 2s at 1000 W. The films processed with microwaves exhibit higher crystallinity and larger average crystalline size, which increases with increasing power, than those processed using a conventional furnace. Additionally, microwaves enable a small increase in pore size and a significant enhancement in the porosity for the mesoporous films. These results demonstrate that microwaves provide a simple methodology to fine tuning the crystallinity and morphology of mesoporous transition metal oxide films.

EXPERIMENTAL SECTION

Materials. Cobalt (II) nitrate hexahydrate ($Co(NO_3)_2 \cdot 6H_2O$) (ACS reagent, ≥98%), citric acid (ACS reagent, ≥99.5%), tetrahydrofuran (THF, contains 250 ppm BHT as inhibitor, ACS reagent, ≥99.0%)，sulfuric acid (ACS reagent, 95.0-98.0%), methoxy poly(ethylene glycol) methacrylate

(PMPEGMA, 475 g·mol^{-1}), n-butyl acrylate (>99%), N,N-dimethylformamide (DMF) (anhydrous, 99.8%) and hexane (anhydrous, 95%) were purchased from Sigma-Aldrich. 2,2-Azobis(isobutyronitrile) (AIBN) (Aldrich, 98%) was purified by recrystallization from methanol and used as the initiator. 4-cyanopentanoic acid dithiobenzoate (CPADB) was synthesized following previous methods and used as the reversible addition-fragmentation chain transfer (RAFT) agent.[43] Hydrogen peroxide (30% w/w) was obtained from BDH Chemicals. Ethanol (200 proof, anhydrous) was purchased from Decon Laboratories, Inc. A Millipore Milli-Q system was used to purify water to 18.2 MΩ·cm. All chemicals were used as received unless noted otherwise. 500 μm thick double-side polished silicon wafers (resistivity=10-20 Ω·cm, Silicon, Inc.) were used as the substrates for the films. Silicon wafers (0.01-0.02 Ω·cm, Silicon, Inc.) were used as substrates for scanning electron microscopy (SEM) cross-section measurements of the Co_3O_4 films processed by furnace heating.

Preparation of Mesoporous Co_3O_4 films. The block copolymer (BCP) template for the mesoporous films was synthesized by RAFT polymerization of methoxy poly(ethylene glycol)methacrylate, followed by butyl acrylate as previously described.[44] The molecular weight of the poly[methoxy poly(ethylene glycol)methacrylate]-block-poly(butyl acrylate). PMPEGMA-b-PBA, was 59 kg/mol with 57.6 wt% PBA as determined by gel permeation chromatography and ^{1}H NMR, respectively.[44] The precursor solution was prepared by dropwise addition of a solution of 0.274 g $Co(NO_3)_2 \cdot 6H_2O$ and 0.090 g citric acid dissolved in 0.9 g ethanol to a solution of 0.2 g PMPEGMA-*b*-PBA dissolved in 2.7 g THF under continuous magnetic stirring at room temperature. The solution was stirred for an additional 12 h before film casting to ensure homogeneity of the solution.

Prior to use, the silicon wafers were cleaned in piranha solution (H_2SO_4: H_2O_2 = 3:1 v/v) at 90 °C for 45 min, rinsed five times with water, and dried with N_2 gas. Films were fabricated using approximately 20 μL of precursor solution by flow-coating[45] at 15 mm/s with a gap height of 200 μm. The films were dried/aged at room temperature for 30 min prior to calcination at 200 ˚C for 1 h in a preheated muffle furnace (Ney Vulcan 3-130) to generate micelle structured cobalt carbonate films. The silicon wafer coated with the cobalt carbonate film was cleaved into ≈1.5 cm × ≈1.5 cm pieces. Microwaves (BP-210, Microwave Research & Applications Inc.) were used to induce the transformation to oxide and removal of the BCP template through energy absorption by the silicon substrate to rapidly heat the films.[46-47] The microwave power (350 W to 1500 W) and time (1 s to 60 s) were systematically varied. As a control, a muffle furnace at 325 ˚C was used for the transformation to oxide and removal of the template instead of microwave heating, but longer heating time (> 5 min) was necessary to obtain mesoporous cobalt oxide films.

Characterization. Fourier-transform infrared spectroscopy (FTIR, Thermo Scientific Nicolet iS50 FTIR spectrometer) with a resolution of 8 cm^{-1} based on the average of 128 scans was used to determine the chemical evolution of the films during calcination. The FTIR measurements were performed in transmission mode with details of the measurements following our prior work examining reaction kinetics in thin films.[48] Briefly, the spectra were obtained under continuous purge gas (dried air, Parker-Balston) and were corrected for the background of the silicon wafer. A standard baseline correction was applied using the OMNIC software (Thermo Scientific Nicolet) to the subtracted data for the spectra presented herein.

Atomic force microscopy (AFM, Dimension ICON, Veeco) in tapping mode using a silicon AFM probe (AppNANO, ACT-200, f= 200-400 kHz, k = 13-77 N/m) probed the surface

morphology of the films. The refractive indices of the films were determined using a variable angle spectroscopic ellipsometer (UV-vis-NIR; 250-1700 nm; VASE M-2000, J.A. Woollam Co.). The ellipsometric angles were fit to a multilayer model consisting of silicon, 10 Å thick interface, 8 Å SiO_2 (based on prior reports for native oxide on silicon),[49] and a general oscillator (GenOsc) model (WVase, J.A. Woollam) using Gaussian and Lorentzian functions to describe the optical properties of the cobalt oxide films.

Ellipsometric porosimetry (EP)[50] was used to determine the mesopore size distribution using toluene as the probe solvent with both adsorption and desorption isotherms measured at a fixed incident angle of 70˚. The relative pressure of toluene (P/P_0) controlled by two mass flow controllers (MSK-146C-FF000-1). The relative volume fraction of the absorbed toluene as a function of P/P_0 was estimated using the Lorentz-Lorenz effective medium approximation. The pore size distribution was determined from the adsorption isotherm using the Kelvin equation.[51] In order to calculate the surface area from the EP measurements, a reference film of cobalt oxide was prepared using the same conditions as the furnace heating sample but without the BCP template in the precursor solution to obtain the partial pressure dependent thickness of adsorbed toluene on cobalt oxide as shown in Figure S1.[52] The surface area was estimated via the *t*-plot method[44, 52-53] assuming the equivalent adsorption behavior for the flat reference surface and mesoporous surface.[52]

The morphology of the mesoporous Co_3O_4 films was assessed using grazing incidence X-ray diffraction (GIXD) and grazing incidence small angle X-ray scattering (GISAXS) on the Complex Materials Scattering (CMS/11-BM) beamline at the National Synchrotron Light Source II (Brookhaven National Laboratory, Upton, NY). The films were illuminated with 13.5 keV

radiation (λ = 0.918 Å) at an incident angle of 0.15°. A line cut along q_r at $q_z = 0.03 \pm 0.01$ Å^{-1} (specular condition) of 2D scattering pattern was used to obtain the 1-D profiles. A clean silicon wafer was used for the background reference and the scattering from silicon was subtracted from the GISAXS data.

The nanostructures associated with the mesoporous Co_3O_4 films were directly visualized using transmission electron microscopy (TEM, FEI Tecnai F20). To prepare the samples for TEM, the films were scraped from silicon wafers and ground using an agate mortar and pestle (Cole-Palmer). The ground mesoporous cobalt oxide powders were dispersed in acetone using an ultrasonic cleaner (VWR 97043-960). A drop of the dispersion was deposited on carbon-coated copper grids (CF200-CU, Electron Microscopy Sciences) and allowed to dry before imaging. Additionally, the mesopore structure was imaged through a cross-section of the Co_3O_4 film using a Quanta 450 FEG instrument with an accelerating voltage of 10 keV. The cross-section sample was prepared simply by cleaving the silicon wafer with the film attached along the Si (100) plane.

Results and discussion

In order to generate templated porous metal oxides from the metal nitrate-citric acid precursors, a thermally stable carbonate framework must form prior to significant degradation of the templating agent.[40-41] The PMPEGMA-b-PBA template begins to decompose at > 250 °C as determined by TGA (Figure S2), while a much lower temperature is required for the conversion of cobalt-nitrate-citric acid complex precursor to cobalt carbonate (~130 °C).[41, 48, 54] The conversion of cobalt nitrate-citric acid complexes to cobalt carbonate at 200 °C without significant degradation of the template was confirmed using FTIR spectroscopy (Figure S3). For the as-cast films that contain the PMPEGMA-b-PBA template and the cobalt nitrate-citric acid complex, the FTIR spectra contain peaks attributed to C-H stretching between 3000 and 2800 cm^{-1} and C=O stretching at 1735

cm^{-1} from the polymeric template and the citric acid as well as two broad peaks at 1450 and 1290 cm^{-1} due to the asymmetric stretching of the coordinated nitrate and the peak at 1050 cm^{-1} due to the symmetric stretching of the coordinated nitrate (to the cobalt).[55-57] After heating the films at 200 °C, these two broad peaks shift from 1450 and 1290 cm^{-1} to 1590 and 1400 cm^{-1}. This shift in wavenumber is consistent with the formation of inorganic (cobalt) carbonates.[41]

Calcination at 325 °C for 45 min generates cobalt oxide and removes the PMPEGMA-b-PBA template based on TGA (Figure S2). These two changes are confirmed by FTIR (Figure S3) where the broad carbonate band between 1600 cm^{-1} and 1320 cm^{-1} and peaks associated with the C=O vibration at 1735 cm^{-1} and C-H stretch between 3000 and 2800 cm^{-1} of the PMPEGMA-b-PBA disappear, while sharp peaks at 661 cm^{-1} and 656 cm^{-1} associated with Co_3O_4 emerge after calcination at 325 °C. Similar FTIR spectra to those obtained from furnace heating at 325 °C for 45 min can be observed with relatively short microwave heating (for example at 600 W for 6 s) of the cobalt carbonate films as shown in Figure S4. This indicates the rapid conversion from cobalt carbonate to cobalt oxide and the removal of the block copolymer template with microwaves in two orders of magnitude less processing time than typically used for calcination of mesoporous materials. These spectra for the cobalt oxide films contain only characteristic peaks from the inorganic compound, which indicate the complete removal of the block copolymer template within the detection limits of the FTIR measurement. This rapid conversion on the heating of the film through the interactions of the microwave with the silicon wafer substrate,[46] which can result in hundreds of degrees temperature rise in the matter of seconds.

Figure 1a illustrates the sensitivity of the film chemistry to the microwave time using 420 W microwaves. For 25 s or less, the FTIR spectra are essentially unchanged, but the spectrum rapidly transitions to indicate complete removal of the template and nearly complete conversion to the

oxide at 26 s. This result suggests that the conversation reaction occurs within 1 s. Additional FTIR spectra for different microwave power are shown in Figures S4. In these each of these cases, there is an abrupt transition from pure carbonate to nearly pure oxide within 1 s. There is however an apparent threshold power requirement to induce this transition. As shown in Figure S5, the conversion of cobalt carbonate into cobalt oxide does not occur within 60 s at microwave power less than 400 W. Even at 3 min at 400 W, there is no evidence for any chemical change in the film. However, upon reaching or exceeding the power of 420 W, complete conversion of cobalt carbonate into cobalt oxide and full removal of block copolymer template occur within 30 s, as shown in Figure 1b. As the microwave power increases, the critical time required for the conversion of cobalt carbonate into cobalt oxide decreases. For example, at the microwave power of 1000 W or 1500 W, this conversion of cobalt carbonate into cobalt oxide occurs within 2 s. It is instructive to compare the conversion kinetics for the microwave processing with that in a preheated furnace. As shown in Figure S6, the conversion from cobalt carbonate to cobalt oxide required 10 min with furnace heating at 325 °C, which confirms the acceleration of the calcination process using microwaves relative to these typical calcination conditions.[41, 48, 54]

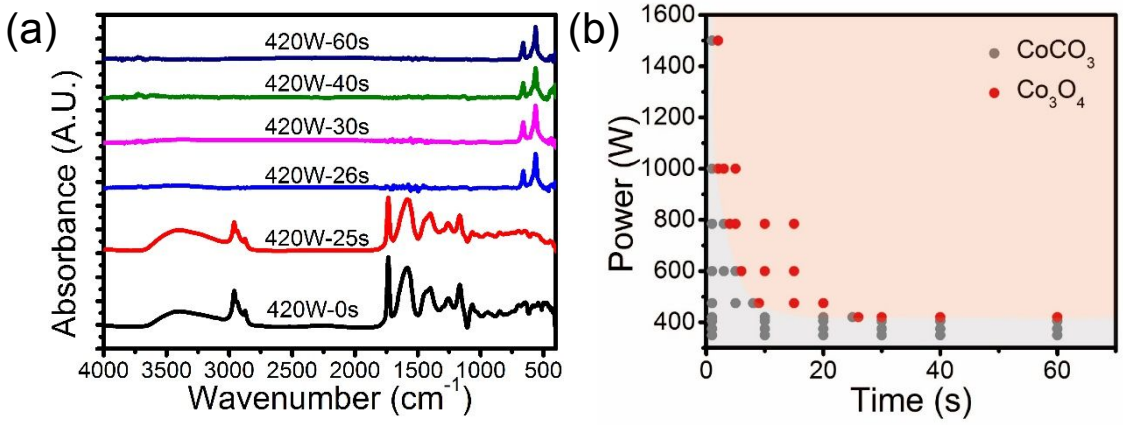

Figure 1. (A) FTIR spectra of templated films after processing with 420 W microwaves for different times. The transformation from cobalt carbonate to cobalt oxide can be clearly distinguished as the microwave time is increased from 25 to 26 s. (B) Influence of microwave power and heating time on the chemical nature of the films.

The nanostructure of the mesoporous cobalt oxide films is dependent on the processing details as shown in Figure 2. The mesopores obtained from the PMPEGMA-b-PBA template are not highly ordered, but there is a common size throughout the micrographs of approximately 15 nm that can be attributed to the mesopores. The sample preparation of the powders for TEM from the films tends to lead to multiple layers of pores and particles as well as stochastic orientation of the structure, so we avoid any quantitative analysis of these TEM images to avoid misinterpretation due to image containing multiple layers. Nonetheless, the limited ordering from the TEM images is consistent with the surface morphology determined by AFM (Figure S7). When comparing the TEM micrographs, the structure of the framework is dependent on the processing details. Heating in the furnace leads to small particles in the framework (Figure 2a). The average particle size appears to increase slightly with microwave processing at 420 W (Figure 2b) in comparison to the furnace calcination. The size of the particles that comprise the framework increases as the power is increased to 785 W (Figure 2c) and 1500 W (Figure 2d). For the highest power examined, the particles appear to have grown to the size of the framework and faceting consistent with crystallization of the Co_3O_4 can be observed in the TEM micrographs (Figure 2d). Interestingly, this film was processed for the shortest period of time (2 s), which suggests extremely rapid crystal growth in the framework with microwaves at high power.

One consequence of the film geometry is that the material is confined by the substrate, which limits contraction in the plane of the film. The stresses developed during calcination tend to result in

uniaxial contraction for block copolymer templated mesoporous materials using conventional heating.[59-60] This uniaxial contraction leads to significant pore shrinkage along the axis oriented perpendicular to the substrate and in some cases collapse of the mesopore structure.[52, 54, 61] To illustrate similar contraction in these Co_3O_4 films, Figure S8 shows a cross-sectional SEM micrograph of Co_3O_4 films produced by furnace heating at 325 °C. The mesoporous cobalt oxide film exhibits asymmetric ellipsoidal pores with major axes of ≈15 nm oriented parallel to the substrate and minor axis of ≈6 nm oriented perpendicular to the substrate. These observations are consistent with anisotropic contraction of the mesostructure that leads to ellipsoidal mesopores.

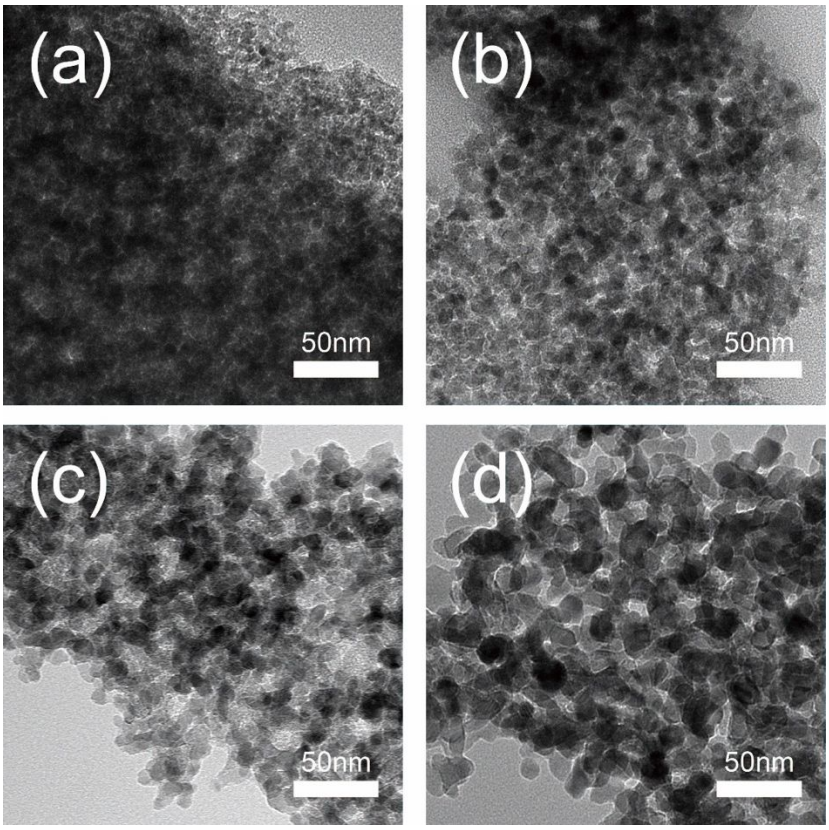

Figure 2. TEM micrographs of mesoporous cobalt oxide films calcined by (a) furnace heating at 325 °C for 10 min or microwave heating at (b) 420 W for 26 s, (c) 785 W for 5 s, and (d) 1500

W for 2 s. The time used is the minimum required to transform to oxide and remove the template for each condition.

As an ordered structure is not readily apparent from the TEM micrographs and these only provide local structural information, the nanostructure of the mesoporous cobalt oxide was further investigated using GISAXS. Figure 3a illustrates the 2D scattering profiles of mesoporous cobalt oxide films calcined in the furnace and with microwaves at 475 W for identical exposures. 2D GISAXS profiles for the other microwave conditions are shown in Figure S9. These scattering profiles are similar with a diffuse spot at finite q_r, associated with in plane correlations, centered at q_z corresponding to the specular condition. A streak extends from this spot in q_z that appear similar to Bragg rod scattering, but no discrete peaks associated with out of plane correlations are observed in any of the scattering patterns. To quantify the in-plane correlations, 1D profiles from a line cut at $q_z = 0.03 \pm 0.01$ Å^{-1} (corresponding to the specular reflection of the beam) are shown in Figure 3b. There is a broad peak associated with the correlation between mesopores for all conditions examined, but no higher order reflections as expected for the limited ordering of the mesopores observed by TEM (Figure 2). There is a quantitative shift in the peak position to lower *q*, indicative of larger spacing, with the microwave processing with the lowest *q* peak position at the highest microwave power.

Figure 3c illustrates how the in-plane *d*-spacing for the mesoporous cobalt oxide films determined from this correlation peak in the line cut depends on the processing conditions. In general, the *d*-spacing is not dependent on the processing time for a given microwave power, which is somewhat unexpected due to the crystallization of the Co_3O_4. The in-plane *d*-spacing for mesoporous cobalt oxide produced by furnace heating is approximately 30 nm. This *d*-spacing of the mesoporous cobalt oxide is increased slightly when using microwaves, ranging from approximately 31.2 to

33.2 nm, depending on the heating power. Larger *d*-spacing is found for higher microwave power. These results suggest that rapid heating (and by inference, conversion to oxide) reduces the volumetric contraction. This effect may be similar that leading to decreased defects in zeolite membranes through rapid thermal processing.[62]

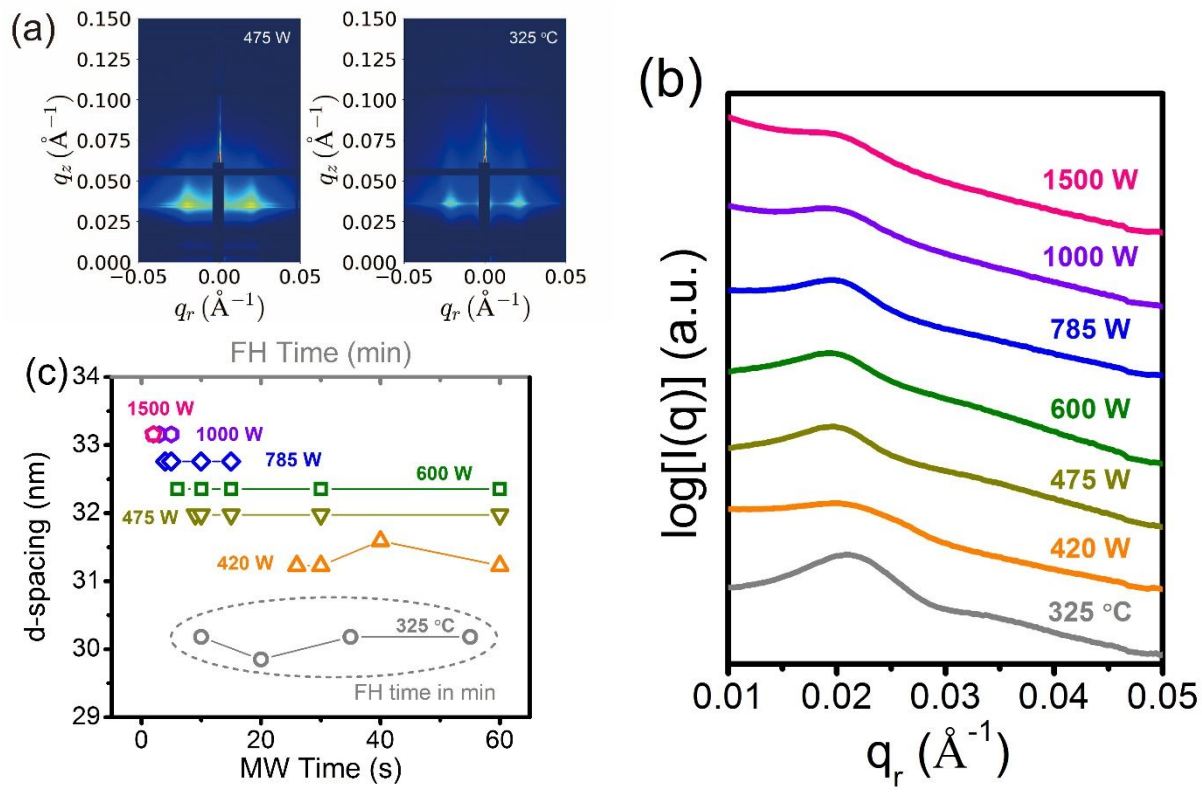

Figure 3. (a) 2-D GISAXS profiles for mesoporous cobalt oxide films fabricated by furnace heating at 325 °C for 10 min and microwave heating at 475 W for 60 s. (b) Comparison of the 1D GISAXS profiles as a function of process condition. The calcination time was the critical (minimum) time to obtain the oxide phase. (c) In-plane *d*-spacing of mesoporous cobalt oxide films prepared using furnace heating (FH) at 325 °C and microwave heating (MW). Note the different time scales for FH and MW methods.

This differences in the structure of the mesoporous cobalt oxide films can be better illustrated through pore texture determined by ellipsometric porosimetry (EP). Figure 4a illustrates the adsorption and desorption isotherms for mesoporous cobalt oxide films prepared by furnace and microwave heating. Figure S10 illustrates these isotherms for other microwave conditions. All of the mesoporous cobalt oxide films exhibit the type IV isotherms with Type H1 hysteresis loop, which are typical of ordered mesoporous materials with spherical pores.[63-64] The hysteresis loop is shifted to higher partial pressure with microwaves (Figure 4a), which should correspond to larger mesopores. As shown in Figure 4b, the pore size distribution for the mesoporous cobalt oxide prepared by calcination in a furnace is nearly Gaussian with an average mesopore size of 2.5 nm, while microwave calcination at 1000 W for 2 s leads to an apparent bimodal pore distribution. The smaller mesopore size appears similar to that of the furnace processed film, but there is a larger mesopore component that is centered at 4.2 nm. This suggests that the rapid calcination by microwaves decreases the contraction experienced by the mesopores, despite the larger apparent particle size from TEM (Figure 2). Due to the anisotropic shape of the mesopores (Figure S8), the pore size estimated from the Kelvin equation (Kelvin radius [r_k]) is nearly the minor axis of the asymmetric ellipsoidal pores due to the mechanism of capillary condensation in the mesopores.[53] Furnace heating at 325 °C leads to an average $r_k \approx 2.5$ nm, which is similar to the minor axis of the corresponding asymmetric ellipsoidal pores (≈3 nm) from cross-sectional SEM micrographs (Figure S8).

Figure S11 illustrates the pore size distributions obtained from the microwave calcination for the different conditions. Porosimetry indicates that there are some smaller (micro)pores, which we attribute to the interstitial space between particles in the walls. As ellipsometric porosimetry has not been established for micropores,[50] we will focus on the mesopores for quantitative analysis. At

low power (420 W), compared to the pore size distribution of the furnace processed film, this distribution broadens and becomes slightly bimodal with an apparent peak at approximately 4.0 nm and a slight shoulder at around 2.4 nm. As the power is increased, the pore size distribution further broadens, but with a clear bimodal distribution. There appear to be two common sizes for the mesopores, approximately 2.4-2.5 and 4.0-4.2 nm, which is suggestive of an interplay between processes. The smaller size is solely obtained with calcination in a furnace, but the fraction of this smaller size grows as the microwave power increases. In addition to the pore size, the details of the processing influence other pore texture properties. Figure 4c illustrates how the porosity of these mesoporous cobalt oxide films, as estimated from V_{ab}/V_{film} at $P/P_0 \approx 1$ with the assumption that all pores are filled, is enhanced using microwave heating compared to those processed using furnace heating. An increase in the microwave power leads an increase in the porosity of the mesoporous films (Figures 4c and S12). Intriguingly, the microwave heating time has little impact on porosity (Figure S13). From the adsorption isotherms, the surface area of the mesoporous films can be estimated using *t*-plots (Figure S14). As shown in Figure 4d, there is a small decrease in the surface area of mesoporous cobalt oxide films fabricated with microwaves relative to more standard furnace calcination. This can be rationalized in terms of the smaller pore size and smaller primary particle size (Figure 2) of the furnace processed films. The surface area of the microwave heated cobalt oxide films is nearly independent of the microwave power.

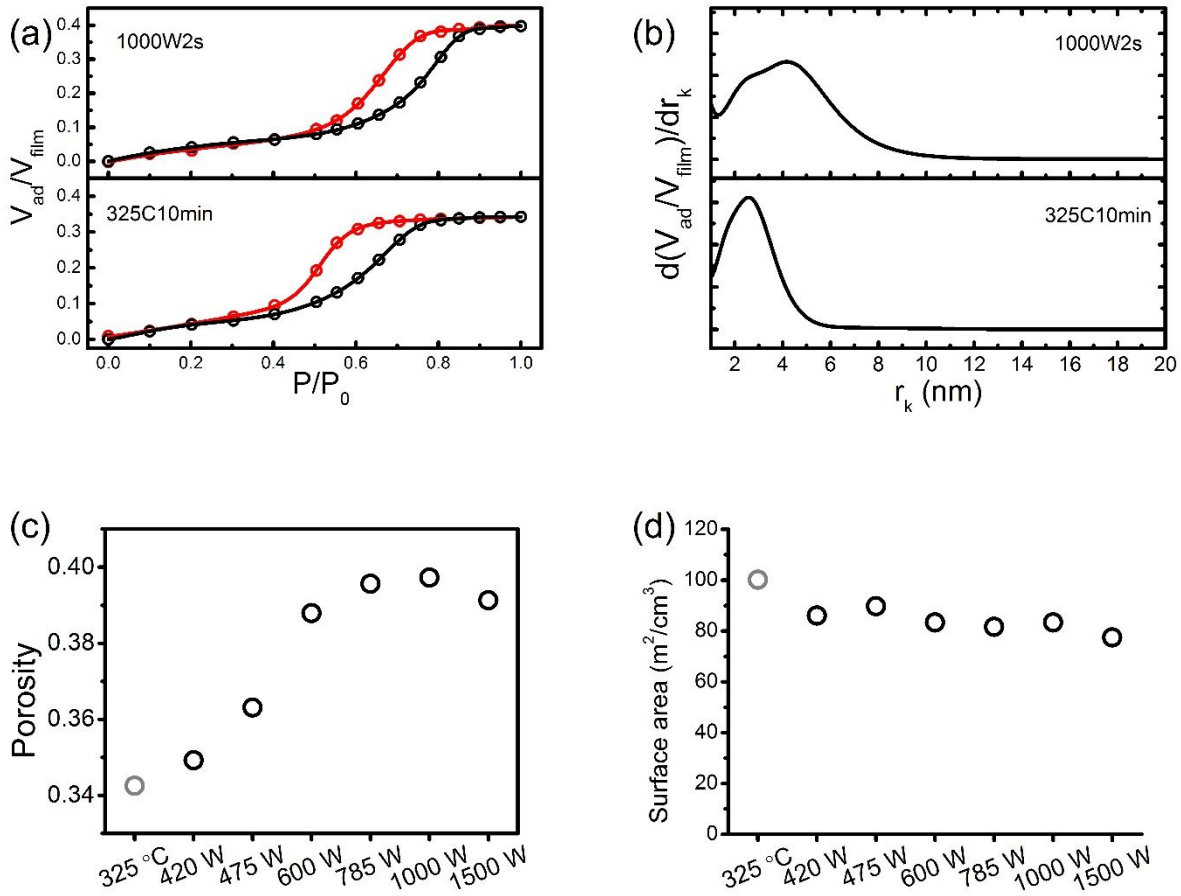

Figure 4. (a) Adsorption (black ○) and desorption (red ○) isotherms for mesoporous cobalt oxide films processed using furnace heating at 325 °C for 10 min and microwave heating at a 1000 W for 2 s from EP and (b) corresponding pore size distribution from the adsorption isotherms using the Kelvin equation. (c) Porosity and (d) surface area of cobalt oxide films calcinated at 325 °C in furnace (gray ○) for 10 min or by microwaves (black ○) as a function of power at the critical time corresponding to the transformation of carbonate to oxide.

GIXD was used to elucidate information about the crystal structure of these cobalt oxide films as a function of processing conditions. Figure 5a illustrates the difference in the GIXD patterns for the furnace and microwave (1000 W for 2 s) calcined mesoporous cobalt oxide films. Despite the much shorter heating time (2 s vs. 10 min), the diffraction peaks associated with cubic Co_3O_4 (PDF

card number: 01-078-1969) are much better developed with microwave heating. This result suggests that the microwaves can dramatically promote crystallization of the Co_3O_4 as the initial film thickness was identical. Figure S15 presents additional GIXD patterns of the microwave processed films. These GIXD data provide clear evidence for the rapid conversion of the carbonate to crystalline oxide: after microwave at 475 W for 8 s, there are no peaks in the diffraction pattern (amorphous cobalt carbonate), which agrees with the FTIR results in Figure S2, but increasing the time by 1 s (475 W for 9 s) leads to well defined diffraction peaks consistent with cubic Co_3O_4. Increasing the microwave heating time to 60 s does not appreciably change the GIXD profile (Figure S15). This observation is counter to furnace heating where the diffraction peaks grow in intensity and sharpen as the calcination time is increased.

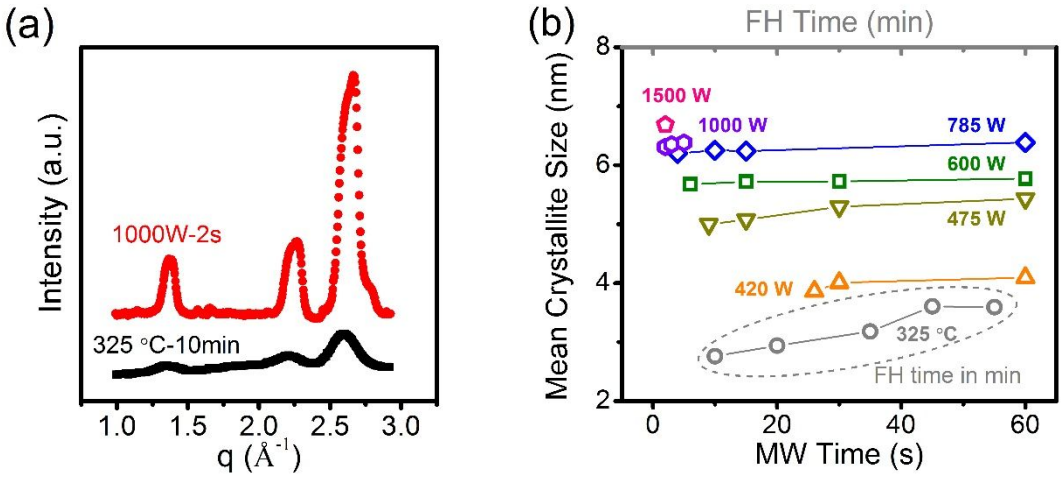

Figure 5. (a) GIXD profiles for microwave heated (black) and conventional furnace heated (red) cobalt oxide films. (b) Average crystallite size of Co_3O_4 films prepared using conventional furnace heating (FH) at 325 °C and microwave heating (MW) at different powers with different heating time. Note the time for FH is in minutes while MW is in seconds.

Examination of the width of the most intense (311) diffraction peak provides some insights into the average size of the Co_3O_4 crystallite from the Scherrer Equation[65-66] assuming a shape factor value of 0.9 (Figure 5b). With the furnace heating process, the average crystallite size of Co_3O_4 is approximately 2.7 nm after 10 min at 325 ºC. Increasing the time from 10 min to 55 min leads to an increase in the crystallite size from 2.7 to 3.6 nm, which is indicative of crystal growth with longer heating time in the furnace. In contrast, microwaves exhibit a much weaker dependence of the average crystal size on heating time. However, the microwave power dramatically influences the average crystal size of Co_3O_4 increasing from approximately 3.9 to 6.7 nm as the microwave power was increased from 420 W to 1500 W. Even at low power, the crystal size from the microwaves (< 60 s) is greater than that obtained using the furnace for 55 min. This dependence of crystallite size of Co_3O_4 on the different heating strategies estimated from the GIXD patterns coincides with the trend of cobalt oxide particle size observed in TEM micrographs, but the average crystal size calculated from the Scherrer equation does not quantitatively match the particles sizes from TEM (Figure 2). This suggests that the particles are polycrystalline, which leads to a lack of a quantitative relationship between d-spacing from GISAXS, average crystal size, pore size observed in TEM micrographs, and Kelvin radius. Due to the anisotropic pore structure, we will briefly describe the consistency in the structural sizes for the different measurements. For an isotropic sample, the *d*-spacing and the sum of the pore and crystal size should be roughly equivalent if the crystal size is approximately the wall thickness. However for the films examined here, contraction of the film perpendicular to the substrate during calcination leads to anisotropy in the mesostructure with ellipsoidal mesopores. The pore size from porosimetry (Kelvin radius) is nominally similar to the minor axis of the asymmetric ellipsoidal pores (from SEM, Figure S8), while the pore size observed in TEM micrographs is consistent with

the major axis of the ellipsoidal pores (from SEM, Figure S8). The GISAXS patterns exhibit defined correlations specifically in the plane of the film, so the d-spacing determined from GISAXS represents the center-to-center distance between mesopores in the plane of the film. This d-spacing is nominally consistent with the sum of the pore size observed in TEM micrographs (~ 15 nm) and the particle size.

Previous studies have suggested that microwave heating process can promote the crystallization by accelerating nucleation and crystal growth.[67-68] However, to understand the dependence of crystallite size on the microwave power, one need to consider which stage of the syntheses between nucleation and crystal growth is selectively accelerated by microwave irradiation. Scheme 1 shows three cases of acceleration in the microwave synthesis: (a) acceleration in both nucleation and crystal growth, (b) acceleration in nucleation only, and (c) acceleration in crystal growth only. Accounting for the thickness of these mesoporous cobalt oxide films and the area of the (311) diffraction peak, the relative crystallinity of the mesoporous cobalt oxide framework on conventional thermal heating at 325 °C and microwave heating at different powers with different processing time can be estimated according to Eq. (1). In this case, the crystallinity is relative to that of the mesoporous cobalt oxide film microwave heated at 1000 W for 5 s (reference).

$$\text{Relative Crystallinity (\%)} = \frac{I_{sample}(311)}{I_{reference}(311)} \times \frac{m_{reference}}{m_{sample}} \times 100\% \qquad (1)$$

where $I_{sample}(311)$ is the intensity of diffraction peak (311) obtained from the sample to be estimated, $I_{reference}(311)$ is the intensity of diffraction peak (311) obtained from the mesoporous cobalt oxide film microwave heated at 1000 W for 5 s, m_{sample} is the mass of the sample to be

estimated, and $m_{reference}$ is the mass of the mesoporous cobalt oxide film microwave heated at 1000 W for 5 s.

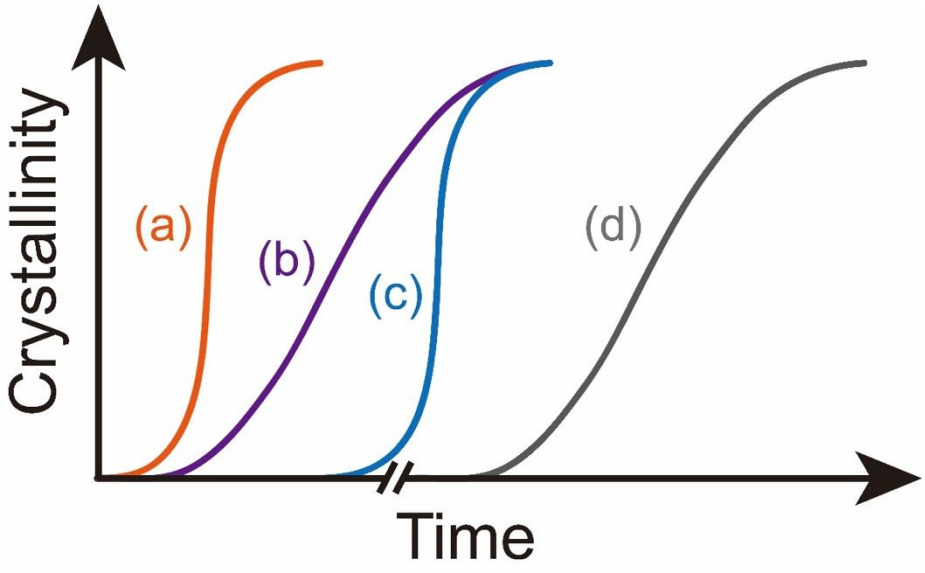

Scheme 1. Dependence of crystallinity of material with heating time representing several modes of microwave irradiation accelerations in the synthesis: (a) nucleation and crystal growth are accelerated, (b) only nucleation is accelerated, (c) only crystal growth is accelerated, and (d) conventional furnace heating without any acceleration.

Figure 6 illustrates the relative crystallization of mesoporous cobalt oxide films as a function of processing strategy. These curves are consistent with the suspected acceleration effect of microwave irradiation on the crystallization of mesoporous cobalt oxide films. These crystallization curves are consistent with acceleration in both the nucleation and crystal growth stages by microwaves. Upon the conversion of cobalt carbonate to cobalt oxide at the critical time, the crystallization exhibits no induction period. Thus, it is difficult to separate the effect of microwave irradiation on nucleation and crystal growth of the cobalt oxide crystals. Nonetheless, these results clearly illustrate the ability to control the relative crystallinity and crystal size using

microwave power, while dramatically decreasing the required reaction time. These concepts could be useful for catalysis and energy applications where the crystal size and facets exposed can dramatically influence performance.

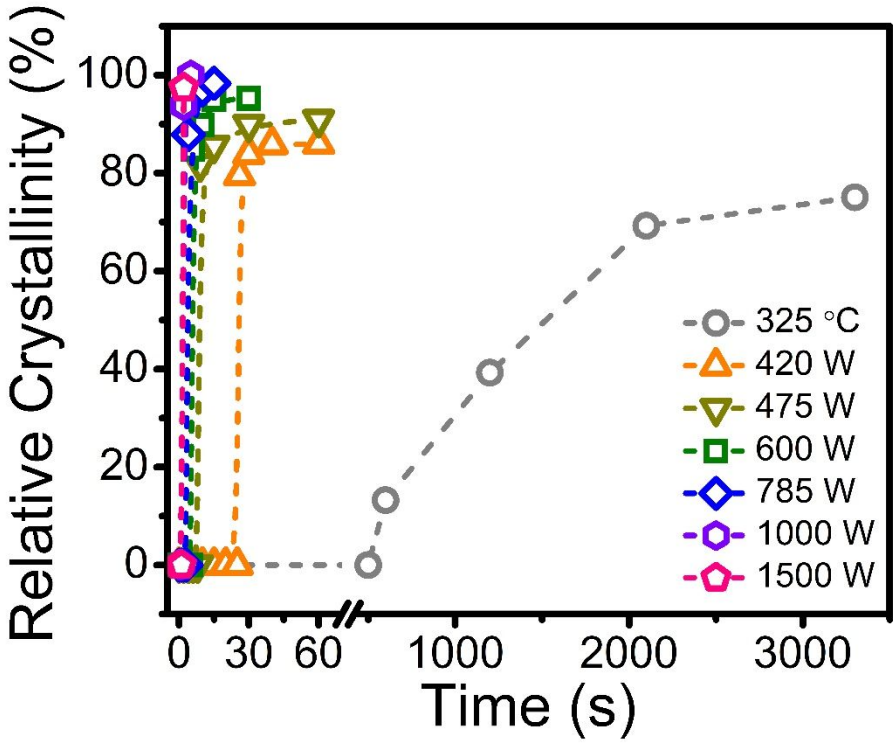

Figure 6. Relative crystallization curves for mesoporous cobalt oxide films using furnace calcination and microwave irradiation at different power. The crystallinity is relative to that obtained when processing for 5 s at 1000 W.

Conclusions

Micelle templated mesoporous cobalt oxide films based on the cooperative assembly of metal nitrate-citric acid and an amphiphilic block copolymer, PMPEGMA-b-PBA, template were fabricated using non-hydrothermal, rapid microwave heating. The microwave power and processing time were systematically investigated for their impact on the composition, morphology

and crystallization of the mesoporous cobalt oxide films. The critical time required for the conversion of cobalt carbonate into cobalt oxide as well as full removal of PMPEGMA-b-PBA template decreases with increasing microwave power with a sharp transition (<1 s required for complete decomposition and conversion). Despite the significantly reduced processing time for microwave heating as compared to the conventional furnace heating, the relative crystallinity is increased and larger average crystal sizes are found. The crystallinity develops rapidly with microwaves with limited growth following the initial conversation to oxide from carbonate (within 1 s). In addition to the crystallinity, the microwaves promote larger average pore size and increased porosity of the mesoporous films as compared to those obtained using furnace heating. This work provides new insights into the potential to use microwaves to readily manipulate the morphology of mesoporous metal oxide films with microwaves.

ASSOCIATED CONTENT

Supporting Information. Additional information including TGA curves, FTIR spectra, AFM images, 2D GISAXS profiles, adsorption and desorption isotherms, pore size distribution, porosity, t-plots from adsorption isotherms, and GIXD patterns. This material is available free of charge via the Internet at http://pubs.acs.org.

AUTHOR INFORMATION

Corresponding Author

* E-mail: bdv5051@psu.edu (B.D.V.)

Author Contributions

The manuscript was written through contributions of all authors. All authors have given approval to the final version of the manuscript.

Notes

The authors declare no competing financial interest.

ACKNOWLEDGMENT

This work was financially supported by the National Science Foundation under Grant No. CBET-1510612. This research used the Complex Materials Scattering (CMS/11-BM) beamline of the National Synchrotron Light Source II, a U.S. Department of Energy (DOE) Office of Science User Facility operated for the DOE Office of Science by Brookhaven National Laboratory under Contract No. DE-SC0012704. The authors express thanks to Dr. Min Gao at Kent State University for assistance with the TEM measurements. The TEM data were obtained at the Liquid Crystal Institute Characterization Facility, Kent State University, supported by the Ohio Research Scholars Program Research Cluster on Surfaces in Advanced Materials.

REFERENCES

1. Beck, J. S.; Vartuli, J. C.; Roth, W. J.; Leonowicz, M. E.; Kresge, C. T.; Schmitt, K. D.; Chu, C. T. W.; Olson, D. H.; Sheppard, E. W.; McCullen, S. B.; Higgins, J. B.; Schlenker, J. L., A new family of mesoporous molecular sieves prepared with liquid crystal templates. *J. Am. Chem. Soc.* **1992,** *114*, 10834-10843.

2. Kresge, C. T.; Leonowicz, M. E.; Roth, W. J.; Vartuli, J. C.; Beck, J. S., Ordered mesoporous molecular sieves synthesized by a liquid-crystal template mechanism. *Nature* **1992,** *359*, 710-712.

3. Sayari, A.; Liu, P., Non-silica periodic mesostructured materials: recent progress. *Microporous Mater.* **1997,** *12*, 149-177.

4. Schuth, F., Non-siliceous mesostructured and mesoporous materials. *Chem. Mater.* **2001,** *13*, 3184-3195.

5. Wan, Y.; Zhao, D., On the controllable soft-templating approach to mesoporous silicates. *Chem. Rev.* **2007,** *107*, 2821–2860.

6. Zhang, J. Y.; Deng, Y. H.; Wei, J.; Sun, Z. K.; Gu, D.; Bongard, H.; Liu, C.; Wu, H. H.; Tu, B.; Schuth, F.; Zhao, D. Y., Design of Amphiphilic ABC Triblock Copolymer for Templating Synthesis of Large-Pore Ordered Mesoporous Carbons with Tunable Pore Wall Thickness. *Chem. Mater.* **2009,** *21*, 3996-4005.

7. Stefik, M.; Mahajan, S.; Sai, H.; Epps, T. H.; Bates, F. S.; Gruner, S. M.; DiSalvo, F. J.; Wiesner, U., Ordered Three- and Five-ply Nanocomposites from ABC Block Terpolymer Microphase Separation with Niobia and Aluminosilicate Sols. *Chem. Mater.* **2009,** *21*, 5466-5473.

8. Vallet-Regi, M.; Ramila, A.; del Real, R. P.; Perez-Pariente, J., A new property of MCM-41: Drug delivery system. *Chem. Mater.* **2001,** *13*, 308-311.

9. Ren, Y.; Ma, Z.; Bruce, P. G., Ordered mesoporous metal oxides: synthesis and applications. *Chem. Soc. Rev.* **2012,** *41*, 4909-4927.

10. Nandi, M.; Mondal, J.; Sarkar, K.; Yamauchi, Y.; Bhaumik, A., Highly ordered acid functionalized SBA-15: a novel organocatalyst for the preparation of xanthenes. *Chem. Commun.* **2011,** *47*, 6677-6679.

11. Vinu, A.; Hossian, K. Z.; Srinivasu, P.; Miyahara, M.; Anandan, S.; Gokulakrishnan, N.; Mori, T.; Ariga, K.; Balasubramanian, V. V., Carboxy-mesoporous carbon and its excellent adsorption capability for proteins. *J. Mater. Chem.* **2007,** *17*, 1819-1825.

12. Nedelcu, M.; Lee, J.; Crossland, E. J. W.; Warren, S. C.; Orilall, M. C.; Guldin, S.; Hüttner, S.; Ducati, C.; Eder, D.; Wiesner, U.; Steiner, U.; Snaith, H. J., Block copolymer directed synthesis of mesoporous TiO2 for dye-sensitized solar cells. *Soft Matter* **2009,** *5*, 134-139.

13. Li, H.-Q.; Liu, R.-L.; Zhao, D.-Y.; Xia, Y.-Y., Electrochemical properties of an ordered mesoporous carbon prepared by direct tri-constituent co-assembly. *Carbon* **2007,** *45*, 2628-2635.

14. Huang, H.-S.; Chang, K.-H.; Suzuki, N.; Yamauchi, Y.; Hu, C.-C.; Wu, K. C.-W., Evaporation-Induced Coating of Hydrous Ruthenium Oxide on Mesoporous Silica Nanoparticles to Develop High-Performance Supercapacitors. *Small* **2013,** *9*, 2520-2526.

15. Wagner, T.; Kohl, C.-D.; Fröba, M.; Tiemann, M., Gas Sensing Properties of Ordered Mesoporous SnO2. *Sensors* **2006,** *6*.

16. Wagner, T.; Waitz, T.; Roggenbuck, J.; Froba, M.; Kohl, C. D.; Tiemann, M., Ordered mesoporous ZnO for gas sensing. *Thin Solid Films* **2007,** *515*, 8360-8363.

17. Waitz, T.; Wagner, T.; Sauerwald, T.; Kohl, C. D.; Tiemann, M., Ordered Mesoporous In2O3: Synthesis by Structure Replication and Application as a Methane Gas Sensor. *Adv. Funct. Mater.* **2009,** *19*, 653-661.

18. Sakatani, Y.; Grosso, D.; Nicole, L.; Boissière, C.; de A. A. Soler-Illia, G. J.; Sanchez, C., Optimised photocatalytic activity of grid-like mesoporous TiO2 films: effect of crystallinity, pore size distribution, and pore accessibility. *J. Mater. Chem.* **2006,** *16*, 77-82.

19. Lu, A. H.; Schuth, F., Nanocasting: A versatile strategy for creating nanostructured porous materials. *Adv. Mater.* **2006,** *18*, 1793-1805.

20. Shi, Y.; Wan, Y.; Zhao, D., Ordered mesoporous non-oxide materials. *Chem. Soc. Rev.* **2011,** *40*, 3854-3878.

21. Chen, Y.; Wu, H. Q.; Gan, S. W.; Wang, Y. H.; Sun, X. L., A hybrid mesoporous membrane synthesized by microwave-assistance: Preparation and characterization. *J. Membr. Sci.* **2012,** *403*, 94-100.

22. Clark, T.; Ruiz, J. D.; Fan, H. Y.; Brinker, C. J.; Swanson, B. I.; Parikh, A. N., A new application of UV-ozone treatment in the preparation of substrate-supported, mesoporous thin films. *Chem. Mater.* **2000,** *12*, 3879-3884.

23. Newalkar, B. L.; Komarneni, S.; Katsuki, H., Rapid synthesis of mesoporous SBA-15 molecular sieve by a microwave-hydrothermal process. *Chem. Commun.* **2000**, 2389-2390.

24. Newalkar, B. L.; Olanrewaju, J.; Komarneni, S., Microwave-hydrothermal synthesis and characterization of zirconium substituted SBA-15 mesoporous silica. *J. Phys. Chem. B* **2001,** *105*, 8356-8360.

25. Hwang, Y. K.; Chang, J. S.; Kwon, Y. U.; Park, S. E., Microwave synthesis of cubic mesoporous silica SBA-16. *Microporous Mesoporous Mater.* **2004,** *68*, 21-27.

26. Chen, S.; Zhao, Y.; Sun, B.; Ao, Z.; Xie, X.; Wei, Y.; Wang, G., Microwave-assisted Synthesis of Mesoporous Co3O4 Nanoflakes for Applications in Lithium Ion Batteries and Oxygen Evolution Reactions. *ACS Appl. Mater. Interfaces* **2015,** *7*, 3306-3313.

27. Chen, G.; Fu, E.; Zhou, M.; Xu, Y.; Fei, L.; Deng, S.; Chaitanya, V.; Wang, Y.; Luo, H., A facile microwave-assisted route to Co(OH)2 and Co3O4 nanosheet for Li-ion battery. *J. Alloys Compd.* **2013,** *578*, 349-354.

28. Gallis, K. W.; Landry, C. C., Rapid Calcination of Nanostructured Silicate Composites by Microwave Irradiation. *Adv. Mater.* **2001,** *13*, 23-26.

29. Tompsett, G. A.; Conner, W. C.; Yngvesson, K. S., Microwave synthesis of nanoporous materials. *ChemPhysChem* **2006,** *7*, 296-319.

30. Wang, H. W.; Kuo, C. H.; Lin, H. C.; Kuo, I. T.; Cheng, C. F., Rapid formation of active mesoporous TiO2 photocatalysts via micelle in a microwave hydrothermal process. *J. Am. Ceram. Soc.* **2006,** *89*, 3388-3392.

31. Le, Z. Y.; Liu, F.; Nie, P.; Li, X. R.; Liu, X. Y.; Bian, Z. F.; Chen, G.; Wu, H. B.; Lu, Y. F., Pseudocapacitive Sodium Storage in Mesoporous Single-Crystal-like TiO2-Graphene Nanocomposite Enables High-Performance Sodium-Ion Capacitors. *ACS Nano* **2017,** *11*, 2952-2960.

32. Smeulders, G.; Meynen, V.; Van Baelen, G.; Mertens, M.; Lebedev, O. I.; Van Tendeloo, G.; Maes, B. U. W.; Cool, P., Rapid microwave-assisted synthesis of benzene bridged periodic mesoporous organosilicas. *J. Mater. Chem.* **2009,** *19*, 3042-3048.

33. Domingues, E. M.; Bion, N.; Figueiredo, F. M.; Ferreira, P., Tuning the acid content of propylsulfonic acid-functionalized mesoporous benzene-silica by microwave-assisted synthesis. *Microporous Mesoporous Mater.* **2016,** *226*, 386-395.

34. Brezesinski, K.; Wang, J.; Haetge, J.; Reitz, C.; Steinmueller, S. O.; Tolbert, S. H.; Smarsly, B. M.; Dunn, B.; Brezesinski, T., Pseudocapacitive Contributions to Charge Storage in Highly Ordered Mesoporous Group V Transition Metal Oxides with Iso-Oriented Layered Nanocrystalline Domains. *J. Am. Chem. Soc.* **2010,** *132*, 6982-6990.

35. Grosso, D.; Soler-Illia, G.; Crepaldi, E. L.; Cagnol, F.; Sinturel, C.; Bourgeois, A.; Brunet-Bruneau, A.; Amenitsch, H.; Albouy, P. A.; Sanchez, C., Highly porous TiO_2 anatase optical thin films with cubic mesostructure stabilized at 700 degrees C. *Chem. Mater.* **2003,** *15*, 4562-4570.

36. Stefik, M.; Song, J.; Sai, H.; Guldin, S.; Boldrighini, P.; Orilall, M. C.; Steiner, U.; Gruner, S. M.; Wiesner, U., Ordered mesoporous titania from highly amphiphilic block copolymers: tuned solution conditions enable highly ordered morphologies and ultra-large mesopores. *J. Mater. Chem. A* **2015,** *3*, 11478-11492.

37. Lokupitiya, H. N.; Jones, A.; Reid, B.; Guldin, S.; Stefik, M., Ordered Mesoporous to Macroporous Oxides with Tunable Isomorphic Architectures: Solution Criteria for Persistent Micelle Templates. *Chem. Mater.* **2016,** *28*, 1653-1667.

38. Lee, J.; Orilall, M. C.; Warren, S. C.; Kamperman, M.; Disalvo, F. J.; Wiesner, U., Direct access to thermally stable and highly crystalline mesoporous transition-metal oxides with uniform pores. *Nat. Mater.* **2008,** *7*, 222-228.

39. Xia, Y.; Qiang, Z.; Lee, B.; Becker, M. L.; Vogt, B. D., Solid state microwave synthesis of highly crystalline ordered mesoporous hausmannite Mn3O4 films. *CrystEngComm* **2017,** *19*, 4294-4303.

40. Eckhardt, B.; Ortel, E.; Polte, J.; Bernsmeier, D.; Görke, O.; Strasser, P.; Kraehnert, R., Micelle-Templated Mesoporous Films of Magnesium Carbonate and Magnesium Oxide. *Adv. Mater.* **2012,** *24*, 3115-3119.

41. Eckhardt, B.; Ortel, E.; Bernsmeier, D.; Polte, J.; Strasser, P.; Vainio, U.; Emmerling, F.; Kraehnert, R., Micelle-Templated Oxides and Carbonates of Zinc, Cobalt, and Aluminum and a Generalized Strategy for Their Synthesis. *Chem. Mater.* **2013,** *25*, 2749-2758.

42. Song, L.; Feng, D.; Fredin, N. J.; Yager, K. G.; Jones, R. L.; Wu, Q.; Zhao, D.; Vogt, B. D., Challenges in Fabrication of Mesoporous Carbon Films with Ordered Cylindrical Pores via Phenolic Oligomer Self-Assembly with Triblock Copolymers. *ACS Nano* **2010,** *4*, 189-198.

43. Thang, S. H.; Chong, Y. K.; Mayadunne, R. T. A.; Moad, G.; Rizzardo, E., A novel synthesis of functional dithioesters, dithiocarbamates, xanthates and trithiocarbonates. *Tetrahedron Lett.* **1999,** *40*, 2435-2438.

44. Wang, S.; Tangvijitsakul, P.; Qiang, Z.; Bhaway, S. M.; Lin, K.; Cavicchi, K. A.; Soucek, M. D.; Vogt, B. D., Role of Amphiphilic Block Copolymer Composition on Pore Characteristics of Micelle-Templated Mesoporous Cobalt Oxide Films. *Langmuir* **2016,** *32*, 4077-4085.

45. Stafford, C. M.; Roskov, K. E.; III, T. H. E.; Fasolka, M. J., Generating thickness gradients of thin polymer films via flow coating. *Rev. Sci. Instrum.* **2006,** *77*, 023908.

46. Jin, C.; Murphy, J. N.; Harris, K. D.; Buriak, J. M., Deconvoluting the Mechanism of Microwave Annealing of Block Copolymer Thin Films. *Acs Nano* **2014,** *8*, 3979-3991.

47. Qiang, Z.; Ye, C. H.; Lin, K. H.; Becker, M. L.; Cavicchi, K. A.; Vogt, B. D., Evolution in Surface Morphology During Rapid Microwave Annealing of PS-b-PMMA Thin Films. *J. Polym. Sci., Part B: Polym. Phys.* **2016,** *54*, 1499-1506.

48. Burroughs, M. C.; Bhaway, S. M.; Tangvijitsakul, P.; Cavicchi, K. A.; Soucek, M. D.; Vogt, B. D., Cooperative Assembly of Metal Nitrate and Citric Acid with Block Copolymers: Role of Carbonate Conversion Temperature on the Mesostructure of Ordered Porous Oxides. *J. Phys. Chem. C* **2015,** *119*, 12138-12148.

49. Herzinger, C. M.; Johs, B.; McGahan, W. A.; Woollam, J. A.; Paulson, W., Ellipsometric determination of optical constants for silicon and thermally grown silicon dioxide via a multi-sample, multi-wavelength, multi-angle investigation. *J. Appl. Phys.* **1998,** *83*, 3323-3336.

50. Baklanov, M. R.; Mogilnikov, K. P.; Polovinkin, V. G.; Dultsev, F. N., Determination of pore size distribution in thin films by ellipsometric porosimetry. *J. Vac. Sci. Technol. B* **2000,** *18*, 1385-1391.

51. Lee, H. J.; Soles, C. L.; Liu, D. W.; Bauer, B. J.; Wu, W. L., Pore size distributions in low-k dielectric thin films from X-ray porosimetry. *J. Polym. Sci., Part B: Polym. Phys.* **2002,** *40*, 2170-2177.

52. Boissiere, C.; Grosso, D.; Lepoutre, S.; Nicole, L.; Bruneau, A. B.; Sanchez, C., Porosity and mechanical properties of mesoporous thin films assessed by environmental ellipsometric porosimetry. *Langmuir* **2005,** *21*, 12362-12371.

53. Bhaway, S. M.; Qiang, Z.; Xia, Y.; Xia, X.; Lee, B.; Yager, K. G.; Zhang, L.; Kisslinger, K.; Chen, Y.-M.; Liu, K.; Zhu, Y.; Vogt, B. D., Operando Grazing Incidence Small-Angle X-ray

Scattering/X-ray Diffraction of Model Ordered Mesoporous Lithium-Ion Battery Anodes. *ACS Nano* **2017,** *11*, 1443-1454.

54. Xia, X.; Bass, G.; Becker, M. L.; Vogt, B. D., Tuning Cooperative Assembly with Bottlebrush Block Co-polymers for Porous Metal Oxide Films Using Solvent Mixtures. *Langmuir* **2019,** *35*, 9572-9583.

55. Dag, Ö.; Alayoğlu, S.; Uysal, İ., Effects of Ions on the Liquid Crystalline Mesophase of Transition-Metal Salt:Surfactant (CnEOm). *J. Phys. Chem. B* **2004,** *108*, 8439-8446.

56. Dag, Ö.; Samarskaya, O.; Tura, C.; Günay, A.; Çelik, Ö., Spectroscopic Investigation of Nitrate−Metal and Metal−Surfactant Interactions in the Solid $AgNO_3/C_{12}EO_{10}$ and Liquid-Crystalline $[M(H_2O)_n](NO_3)_2/C_{12}EO_{10}$ Systems. *Langmuir* **2003,** *19*, 3671-3676.

57. Karakaya, C.; Türker, Y.; Dag, Ö., Molten-Salt-Assisted Self-Assembly (MASA)-Synthesis of Mesoporous Metal Titanate-Titania, Metal Sulfide-Titania, and Metal Selenide-Titania Thin Films. *Adv. Funct. Mater.* **2013,** *23*, 4002-4010.

58. Zhang, Y.; Bhaway, S. M.; Wang, Y.; Cavicchi, K. A.; Becker, M. L.; Vogt, B. D., Rapid (<3 min) microwave synthesis of block copolymer templated ordered mesoporous metal oxide and carbonate films using nitrate–citric acid systems. *Chem. Commun.* **2015,** *51*, 4997-5000.

59. Grosso, D.; Balkenende, A. R.; Albouy, P. A.; Ayral, A.; Amenitsch, H.; Babonneau, F., Two-Dimensional Hexagonal Mesoporous Silica Thin Films Prepared from Block Copolymers: Detailed Characterization and Formation Mechanism. *Chem. Mater.* **2001,** *13*, 1848-1856.

60. Yang, H.; Coombs, N.; A. Ozin, G., Thickness control and defects in oriented mesoporous silica films. *J. Mater. Chem.* **1998,** *8*, 1205-1211.

61. Bhaway, S. M.; Kisslinger, K.; Zhang, L.; Yager, K. G.; Schmitt, A. L.; Mahanthappa, M. K.; Karim, A.; Vogt, B. D., Mesoporous Carbon–Vanadium Oxide Films by Resol-Assisted, Triblock Copolymer-Templated Cooperative Self-Assembly. *ACS Appl. Mater. Interfaces* **2014,** *6*, 19288-19298.

62. Choi, J.; Jeong, H. K.; Snyder, M. A.; Stoeger, J. A.; Masel, R. I.; Tsapatsis, M., Grain Boundary Defect Elimination in a Zeolite Membrane by Rapid Thermal Processing. *Science* **2009,** *325*, 590-593.

63. Cychosz, K. A.; Guo, X.; Fan, W.; Cimino, R.; Gor, G. Y.; Tsapatsis, M.; Neimark, A. V.; Thommes, M., Characterization of the Pore Structure of Three-Dimensionally Ordered Mesoporous Carbons Using High Resolution Gas Sorption. *Langmuir* **2012,** *28*, 12647-12654.

64. Sing, K. S. W., Reporting physisorption data for gas/solid systems with special reference to the determination of surface area and porosity (Recommendations 1984). *Pure Appl. Chem.* **2009,** *57*, 603-619.

65. Patterson, A. L., The Scherrer Formula for X-Ray Particle Size Determination. *Phys. Rev.* **1939,** *56*, 978-982.

66. Xia, X.; Qiang, Z.; Bass, G.; Becker, M. L.; Vogt, B. D., Morphological control of hydrothermally synthesized cobalt oxide particles using poly(vinyl pyrrolidone). *Colloid Polym. Sci.* **2019,** *297*, 59-67.

67. Jhung, S. H.; Jin, T.; Hwang, Y. K.; Chang, J.-S., Microwave Effect in the Fast Synthesis of Microporous Materials: Which Stage Between Nucleation and Crystal Growth is Accelerated by Microwave Irradiation? *Chem. - Eur. J.* **2007,** *13*, 4410-4417.

68. Serrano, D. P.; Uguina, M. A.; Sanz, R.; Castillo, E.; Rodríguez, A.; Sánchez, P., Synthesis and crystallization mechanism of zeolite TS-2 by microwave and conventional heating. *Microporous Mesoporous Mater.* **2004,** *69*, 197-208.

For Table of Contents only